Thermal Contribution to the Spin-Orbit Torque in Metallic-Ferrimagnetic Systems

Thai Ha Pham,[1] S.-G. Je,[1,2] P. Vallobra,[1] T. Fache,[1] D. Lacour,[1] G. Malinowski,[1] M. C. Cyrille,[3] G. Gaudin,[2] O. Boulle,[2] M. Hehn,[1] J.-C. Rojas-Sánchez,[1,*] and S. Mangin[1]

[1]*Institut Jean Lamour, CNRS UMR 7198, Université de Lorraine, F-54011 Nancy, France*
[2]*CNRS, SPINTEC, F-38000 Grenoble, France*
[3]*Leti, Technology Research Institute, CEA, F-38000 Grenoble, France*

(Received 21 November 2017; revised manuscript received 17 March 2018; published 20 June 2018)

Two important goals for emerging spintronic applications exploiting current-induced magnetization switching are reducing the critical current to switch the magnetization and reducing or eliminating the need for an external in-plane magnetic field for deterministic magnetization reversal. Here, we present experimental studies of the heavy-metal-ferrimagnetic bilayer system, W/Co_xTb_{1-x} characterized using magnetometry and anomalous Hall resistance measurements for temperatures ranging from 10 to 350 K. The current-induced-switching experiments are performed in the spin-orbit torque geometry where the current pulses are injected in plane and the magnetization reversal is detected by the measurement of the Hall resistance. The full magnetization reversal has been observed in all samples. Despite its large perpendicular magnetic anisotropy we find magnetic reversal for a strongly reduced in-plane magnetic field which is due to thermal contribution to switching. We find a characteristic switching temperature T_{switch} induced by Joule heating which is above the magnetic, $T_{M\,\text{comp}}$, and angular, $T_{A\,\text{comp}}$, compensation temperatures but below its Curie temperature.

DOI: 10.1103/PhysRevApplied.9.064032

I. INTRODUCTION

Spin-orbit torque switching with perpendicularly magnetized material in Hall bar-based devices offers a simple and powerful geometry to probe current-induced magnetization reversal and had opened an alternative way to manipulate magnetization at the nanoscale. The underlying physics is quite rich and complex including the origin of spin-orbit torque (SOT), interfacial effects, and thermal contributions. Magnetization switching by SOT was first observed in heavy-metal-ferromagnetic, HM-FM, ultrathin films [1–3]. The torque is mainly related to the spin Hall effect (SHE) [4–10], where the charge current flowing in the heavy metal is converted into a vertical spin current due to the large spin-orbit coupling. This spin current is then transferred to the FM magnetization, which leads to a torque, namely the spin-orbit torque. It has been demonstrated, for instance, using Pt [4–9], Ta [9–12], W [13–16] as HM and FM layers with perpendicular magnetization like (Co,Fe)B [7,9–12,14,15], Co [4–6], (Co,Fe)Al [16], or (Co/Ni) [8] multilayers. Interface effects can play a key role in the SOT, in particular, interfacial spin memory loss [17] and spin transparency [18], which affects the transmitted spin. Furthermore, additional charge-to-spin current conversion can also occur due to the Edelstein effect [19] in Rashba [20] and topological insulator interfaces [19]. There have been some attempts to unify a model [21–23], including the aforementioned effects. It might be also an interfacial DMI (Dzyaloshinskii-Moriya interaction) which favors the formation of the chiral Neel domain wall [24]. It was shown in FM-HM systems that the reversal of the magnetization occurs first by a magnetic domain nucleation followed by a domain-wall propagation thanks to the SHE and interfacial DMI [8,25–28]. The thermal contribution starts to be considered in those experiments [6,29].

For possible applications the critical switching current needs to be reduced while maintaining a sufficient thermal stability. In the literature, the critical current density to reverse the magnetization J_{CC} is typically of the order of approximately 10^{10} to 10^{12} A/m^2, depending on the applied current pulse duration and on the in-plane external magnetic field [4,5,8,30]. J_{CC} is proportional to the magnetization times the thickness of the FM layer ($J_{CC} \propto Mt_F$). Recently, transition-metal—rare-earth TM-RE ferrimagnetic materials started to attract large attention for spin-orbitronics applications [31–36]. In these ferrimagnetic alloys the net magnetization is given by the sum of the magnetization of the two magnetic sublattices (rare earth and transition metal), which are antiferromagnetically coupled. A key benefit of ferrimagnetic materials is that its net magnetization M can be tuned by changing its composition or temperature [37]. As a result, a magnetic compensation point with zero magnetization can occur for a certain alloy concentration $x_{M\,\text{comp}}$, or temperature, $T_{M\,\text{comp}}$,

*juan-carlos.rojas-sanchez@univ-lorraine.fr

where the magnetization of both sublattices compensates. Moreover, TM-RE thin films are characterized by a large bulk magnetic anisotropy perpendicular to the film plane, which make it easier to integrate TM-RE with different HM materials while keeping large thermal stability [38]. Furthermore, the control of magnetization switching using the ultrafast femtosecond laser pulse has been demonstrated recently for various TM-RE materials [39,40]. Those features are encouraging to combine the control of magnetization by both optical and electrical means. Concerning the spin-orbit torque (SOT) switching, reports on experiments with TM-RE alloys claim that the spin-orbit torque efficiency reaches a maximum at the magnetic compensation point [31–36], however, the critical current is not minimum at this point as might be expected if such critical current would be proportional to net magnetization [33,35,36]. Indeed, we have shown that it is proportional to the perpendicular anisotropy H_k [41]. In this study we address the SOT-switching experiments on well-characterized $//\mathrm{W}/\mathrm{Co}_x\mathrm{Tb}_{1-x}/\mathrm{Al}$ systems for various concentrations. The double // stands for the position of the substrate. We demonstrate that thermal effects are keys to explaining the current-induced magnetization reversal in this system. When the current is injected in the bilayer the Joule heating leads to a large increase of the sample temperature. Using systematic SOT measurements at different temperatures and alloy compositions, we establish that for each concentration x the current-induced magnetization switching occurs for a unique sample temperature $T_{\mathrm{switch}}(x)$. T_{switch} scales with the Curie temperature (T_C) of the alloy. Those findings open room to explore the combination of SOT and thermal contribution towards reducing critical current density to reverse M and, consequently, low power-consumption applications. In the specific case where T_{switch} is close to $T_{M\,\mathrm{comp}}$ an unexpected "double switching" is observed.

II. BASIC CHARACTERIZATION

To study SOT magnetization switching in RE-TM alloys, a model system composed of $\mathrm{Co}_x\mathrm{Tb}_{1-X}$ ferrimagnetic alloys deposited on a tungsten heavy metal with high charge-to-spin conversion efficiency [13] is considered. The samples are grown by dc magnetron sputtering on thermally oxide Si substrates (Si-SiO_2). The full stacks of the samples are Si-SiO_2//W(3 nm)/$\mathrm{Co}_x\mathrm{Tb}_{1-x}$(3.5 nm)/Al(3 nm), with $0.71 \leq \mathrm{x} \leq 0.86$. The 3-nm-thick Al (naturally oxidized and passivated after the deposition) is used to cap the ferrimagnetic layer. The W and CoTb layers have amorphous structure as will be discussed in Sec. IV. As described in the Introduction, ferrimagnetic alloys like CoTb can show a compensation point at which the Co and Tb moments cancel each other, resulting in zero net magnetization. When the net magnetization of the alloy is parallel (respectively, antiparallel) to the magnetization of the terbium sublattice the alloy will be called terbium rich (respectively, cobalt rich). The samples are characterized by a superconducting-quantum-interference-device—(SQUID) VSM magnetometer and magneto-optically Kerr effect (MOKE) at room temperature. The SQUID measurements obtained at room temperature are presented in Fig. 1(a). Magnetization compensation is observed for a concentration $x_{M\,\mathrm{comp}} = 0.77$, where the coercivity H_c diverges and the net saturation magnetization M_s tends to zero. This value is close to the one reported for bulk and thicker $\mathrm{Co}_x\mathrm{Tb}_{1-x}$ films [37,42] at room temperature. Additionally to the divergence of H_c, MOKE measurements show that the Kerr angle rotation changes its sign between Co-rich and Tb-rich samples, which can be explained by the fact that the Kerr signal is mainly sensitive to the cobalt sublattice when a red laser is used [43] (see, for instance, Fig. S1 in the Supplemental Material [44]). Both SQUID and MOKE results clearly show that all CoTb films studied have a strong out-of-plane magnetic anisotropy.

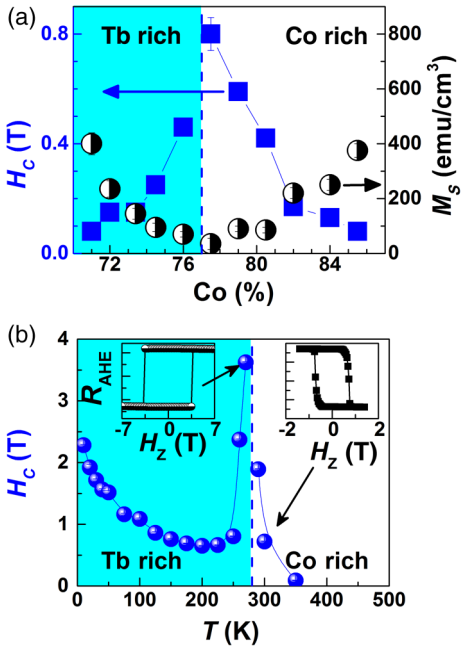

FIG. 1. $//\mathrm{W}(3)/\mathrm{Co}_x\mathrm{Tb}_{1-x}(3.5)/\mathrm{Al}(3)$: (a) Coercive field H_c and saturation magnetization M_s obtained by SQUID measurements vs cobalt concentration at room temperature. Magnetic compensation is observed for $x_{M\,\mathrm{comp}} \sim 0.77$. (b) Temperature dependence of coercivity on Hall bar for $x = 0.78$ showing that $T_{M\,\mathrm{comp}} \sim 280$ K for $x = 0.78$. Insets show the Hall resistance cycle for a temperature below (left) and above (right) $T_{M\,\mathrm{comp}}$. The change of field-switching polarity (FSP) shows evidence that R_{AHE} is mainly sensitive to the magnetization of the cobalt sublattice. H_c at 350 K is 90 mT.

To study spin-orbit-torque switching, the stacks are patterned by standard UV lithography into microsized Hall crosses with a channel of 2, 4, 10, and 20 μm. The results shown are obtained for a width of 20 μm unless otherwise specified. Ti(5)/Au(100) Ohmic contacts are defined by evaporation deposition and the lift-off method

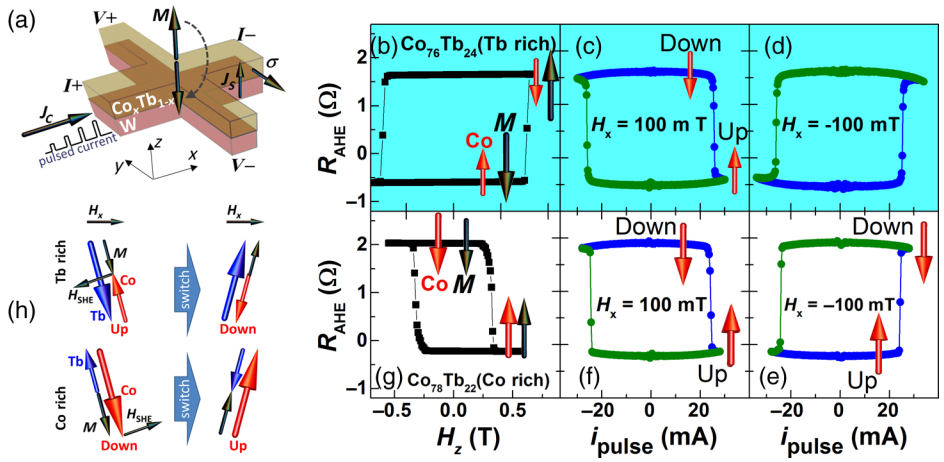

FIG. 2. Anomalous Hall effect and current-induced magnetization reversal at room temperature on Si-SiO_2//W(3)/Co_xTb_{1-x}(3.5)/Al(3). (a) Scheme of the Hall bar along with geometry used. The spin polarization σ is along the y axis. (b),(g) Sweeping perpendicular field ($H\|z$) with a low dc bias of 400 μA. (c)–(f) Sweeping in-plane current ($i_{\rm pulse}\|x$) with an in-plane field $H_x = \pm 100$ mT. The width of the channel current is 20 μm. The current-switching polarity (CSP) for $H_x > 0$ is down-up for Co-rich and Tb-rich samples (c),(f). The CSP in (c) is opposite than predicted for Tb-rich samples as shown in the schematic in (h). The perpendicular effective torque field $\boldsymbol{H}_{\rm SHE}$ is proportional to $\boldsymbol{m} \times \boldsymbol{\sigma}$ and should lead to a change of the sign in the $R_{\rm AHE}(i)$ cycle when changing from the Co-rich to the Tb-rich phase.

on top of W layers. By measuring the anomalous Hall resistance $R_{\rm AHE}$ of the Hall crosses while sweeping the external perpendicular magnetic field H_z at different temperatures, we could determine the magnetic compensation temperature of the samples. Figure 1(b) shows the temperature dependence of H_c for 78% of Co. The coercive field H_c diverges around 280 K, which determines $T_{M\,\rm comp}$ for this composition. Moreover, we can observe in the insets that the $R_{\rm AHE}(H_z)$ cycle is reversed for Tb-rich ($T < 280$ K) and Co-rich ($T > 280$ K) phases, namely change of field-switching polarity (FSP). The latter is due to the fact the anomalous Hall resistance is sensitive to the cobalt sublattice. van der Pauw resistivity measurements leads to a resistivity of W in Si-SiO_2//W(3 nm)/MgO(3 nm) of $\rho_{\rm W} = 162$ $\mu\Omega$ cm. Then we could deduce the $Co_{0.72}Tb_{0.28}$ resistivity $\rho_{\rm CoTb} = 200$ $\mu\Omega$ cm which decreases to 135 $\mu\Omega$ cm when the cobalt concentration reaches $Co_{0.86}Tb_{0.14}$ in accord with previous results [45]. Despite this trend, the amplitude of $R_{\rm AHE}(H_z)$, $\Delta R_{\rm AHE}$, increases as a function of the Co concentration verifying that $R_{\rm AHE}$ is mainly sensitive to the cobalt sublattice (see also Fig S2 [44]).

III. THERMALLY ASSISTED AND SPIN-ORBIT TORQUE SWITCHING

Figure 2(a) shows a scheme of a Hall bar along with the conventions used for current injection, voltage probe, and directions axes. Typical $R_{\rm AHE}(H_z)$ cycles obtained at room temperature with a low in-plane dc current of 400 μA (charge current density of about 2.4×10^9 A/m^2 flowing in each layer) for a Tb-rich (respectively, Co-rich) sample is shown in Fig. 2(b) [respectively, Fig. 2(g)]. As expected, a change of FSP is observed since the alloy net magnetization is parallel to the magnetization of the cobalt sublattice in one case and antiparallel in the other. For the same samples the current-induced switching cycles are shown in Figs. 2(c)–2(d) (Tb rich) and Figs. 2(e) and 2(f) (Co rich) with an in-plane bias field of $H_x = 100$ mT [Figs. 2(c) and 2(f)] and -100 mT [Figs. 2(d) and 2(e)]. The current injection is performed with a pulse duration of 100 μs using a K6221 source coupled to a K2182 Keithley nanovoltmeter. The Hall voltage is measured during the pulse. We have observed the current-induced magnetization switching in all the samples for $0.72 \le x \le 0.86$. The Hall resistance amplitudes are the same for the current-switching and the field-switching cycles indicating that the reversal of magnetization is fully achieved in both cases. The data of the full series are shown in Fig. S3 [44]. Sharp current switching is observed and the critical current reduces when H_x increases following similar trends as that for ferromagnetic materials [30] as shown in Fig. S4. Remarkably, we observe a full magnetization reversal even for an in-plane field H_x as low as 2 mT. The role of the in-plane field can be understood as the field to balance the interfacial DMI to propagate domain walls which have in-plane magnetization after nucleation of magnetic domains or the field to break the symmetry and to allow for a deterministic switching [8,30]. If the SOT depends on the Co moment, the SOT acts as an effective field $\boldsymbol{H}_{\rm SHE} \propto \boldsymbol{m} \times \boldsymbol{\sigma}$ [24,46], where $\boldsymbol{m}$ is the magnetic moment and $\boldsymbol{\sigma}$ the spin polarization of the spin current J_s injected from the W layer into the CoTb layer. $\boldsymbol{\sigma}$ is along the **y** direction in our measurement geometry (it changes between $+y$ and $-y$ when the direction of the injected current is inverted). $\boldsymbol{m}$ changes its sign upon the change of the in-plane field direction. Then the sign of

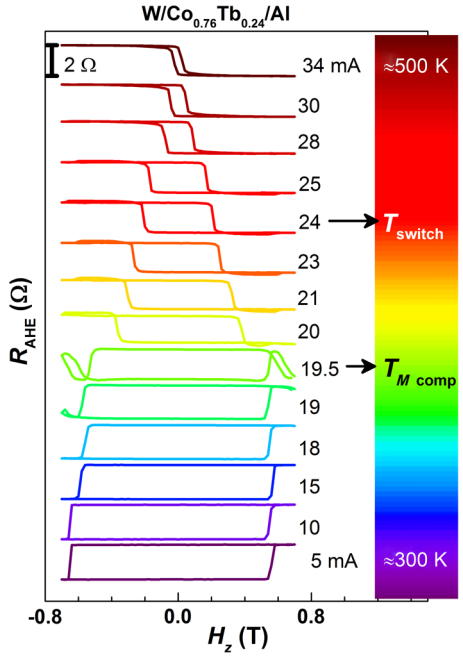

FIG. 3. $R_{\mathrm{AHE}}(H_z, i_{\mathrm{pulse}})$ cycles on Si-SiO_2//W(3)/$Co_{0.76}Tb_{0.24}$(3.5)/Al(3) Hall bar measured at room temperature. The cycles are vertically offset for clarity. It is observed that for $i <$ 19.5 mA the cycle has a signature corresponding to the Tb-rich phase according to our convention. However, for $i >$ 19.5 mA the cycle changes their sign and now corresponds to the Co-rich phase. It is an evidence of the Joule heating effect when high pulse current is applied. 19.5 mA roughly corresponds to $T_{M\,\mathrm{comp}}$. The critical current for this device is about 24 mA. Thus, during the electrical switching $T_{\mathrm{device}} > T_{M\,\mathrm{comp}} > 300$ K for this $Co_{0.76}$ system.

the Hall cycle vs current, $R_{\mathrm{AHE}}(i)$, is reversed when H_x is reversed as observed in Figs. 2(c)–2(f). Additionally, in ferrimagnetic alloys, the effective field $\boldsymbol{H}_{\mathrm{SHE}}$ can be reversed if a Co-rich sample is replaced by a Tb-rich one [a schematic is shown in Fig. 2(h) for $H_x > 0$ and $i > 0$]. The identical effect will be observed if the same sample is kept and the magnetic compensation temperature is crossed. The fact that the samples which have been identified as Co rich and Tb rich at room temperature are showing the same current-switching polarity [Figs. 2(c) and 2(f)] can only be understood if the so-called Tb-rich sample has crossed compensation to become Co rich. This compensation crossing is due to the Joule heating effect. This assumption is tested by measuring $R_{\mathrm{AHE}}(H_z)$ cycles for different applied current pulses on the "Tb-rich" sample shown in Fig. 3. We observe that for applied currents $i <$ 19.5 mA the sign of the cycle demonstrates a Tb-rich nature, however for current $i >$ 19.5 mA the $R_{\mathrm{AHE}}(H_z)$ cycles are reversed and demonstrate a "Co-rich" nature. This is clear experimental evidence that for current close to 19.5 mA the device reaches the sample compensation temperature ($T_{M\,\mathrm{comp}} \sim 320$ K). This demonstrates that the sample is strongly heated during the current-switching experiments. The temperature can be determined by the resistance value as explained in the next section. In Fig. 3 the corresponding temperature is shown using a color code. We can determine that a temperature of 460 K is reached for 24 mA, which is the critical current to switch M [Fig. 2(c)]. This current switching of 24 mA is then obtained for a temperature above $T_{M\,\mathrm{comp}}$, which explains why the sign of the $R_{\mathrm{AHE}}(i)$ cycle is the one expected for a Co-rich sample. We have performed $R_{\mathrm{AHE}}(H_z)$ cycles with an intensity current pulse as high as 34 mA (approximately 525 K), where we can observe that the device shows a ferromagnetic hysteresis loop and remains perpendicularly magnetized. T_C is then higher than 525 K.

IV. CHARACTERISTIC TEMPERATURES OF SWITCHING

Since we have addressed the reason of the observed switching polarity, several questions arise: (i) How much are the devices heated when the switching occurs? (ii) Does the temperature at which the switching occurs change with the initial temperature (temperature at which the experiment is carried out, T_{cryostat})? (iii) How does the switching current and switching temperature depend on composition? (iv) What is the physical meaning of this switching temperature: Angular compensation temperature $T_{A\,\mathrm{comp}}$? In order to address all of those questions we have performed a series of temperature dependence experiments for various samples.

Figure 4(a) shows the $R_{\mathrm{AHE}}(i_{\mathrm{pulse}})$ cycles for $H_x > 0$ at a different cryostat temperature for $W/Co_{0.73}Tb_{0.27}$ (Tb rich at room temperature). We observe the down-up current-switching polarity at 300 K. For 150 K $\leq T_{\mathrm{cryostat}} \leq$ 250 K a double-current-switching loop is observed. This type of double current switching can be explained when the switching temperature is close to $T_{M\,\mathrm{comp}}$ and its origin will be discussed later in the paper [Fig. 4(a) shows only the case of 150 K for clarity]. For 10 K $\leq T \leq$ 100 K we observe only down-up current-switching polarity (we didn't increase too much the pulse current to avoid burning the device). One can calibrate the real sample temperature at a different pulse current by performing the following protocol: (i) measuring the resistance of the current channel $R_{\mathrm{channel}}(i_{\mathrm{pulse}})$ as a function of pulse-current intensity as shown in Fig. 4(b) for different cryostat temperatures, and (ii) measuring the temperature dependence of the current channel $R_{\mathrm{channel}}(T)$ as shown in Fig 4(c) (for which we use a very low dc bias current of only 400 μA). Interestingly, we observe that for Co-rich current-switching polarity (down-up) the device reaches the same resistance (1.373 KΩ) and, consequently, the same switching temperature $T_{\mathrm{switch}} = 435$ K $\pm$ 25 K for this $W/Co_{0.73}Tb_{0.27}$. We note that the resistance decreases when T increases, which is a feature and confirmation of amorphous materials [47]. We have performed the same protocol for various

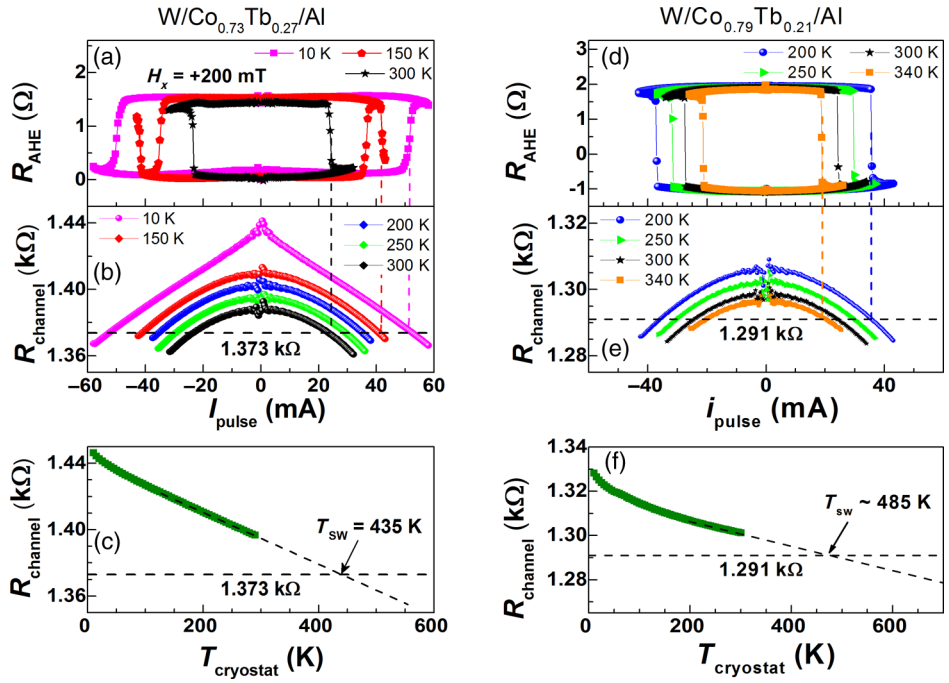

FIG. 4. (a) $R_{\mathrm{AHE}}(i_{\mathrm{pulse}})$ at different cryostat temperatures. Cycles for $x = 0.73$ (Tb rich at room temperature). (b) $R_{\mathrm{channel}}(i_{\mathrm{pulse}})$, and (c) $R_{\mathrm{channel}}(T)$ at different cryostat temperatures. The vertical dashed line points out the critical current to reverse M. It is observed that independently of the initial temperature, the device always reaches the same value of longitudinal resistance (1373 Ω), which means it reaches the same temperature. The linear extrapolation of $R_{\mathrm{channel}}(T)$ allows us to know the temperature corresponding to the current-induced magnetization reversal. Such a temperature is defined as T_{switch}. $R_{\mathrm{channel}}(T)$ is performed with a low bias current of 400 μA. For $Co_{0.73}$ we find that $T_{\mathrm{switch}} = 435\ \mathrm{K} \pm 25\ \mathrm{K}$. (d) $R_{\mathrm{AHE}}(i_{\mathrm{pulse}})$ cycles for $x = 0.79$ (Co rich at room temperature) at different cryostat temperatures. (e) $R_{\mathrm{channel}}(i_{\mathrm{pulse}})$, and (f) $R_{\mathrm{channel}}(T)$ at different cryostat temperatures. It is also observed that independently of the initial temperature, the device always reaches the same resistance, thus it is the same temperature. In this case it corresponds to 1291 Ω and $T_{\mathrm{switch}} \sim 485$ K.

compositions and different devices. An example for the Co-rich sample at room temperature is shown in Figs. 4(d)–4(f) ($W/Co_{0.79}Tb_{0.21}$), where we also observe that the critical current heats up the device to the same channel resistance [Fig. 4(e)], so the same T_{switch} (approximately 485 K for this $Co_{0.79}Tb_{0.21}$ sample), irrespective of the initial temperature. Moreover, on this particular sample $T_{M\,\mathrm{comp}}$ is about 240 K and we observe no change of current-switching polarity (CSP) even for T as low as 10 K, which is well below its $T_{M\,\mathrm{comp}}$.

Additionally, to the characteristic T_{switch} we have just discussed, one can also investigate the temperature dependence of the critical current as shown in Fig. 5(a) for a $Co_{0.79}Tb_{0.21}$ sample (Co rich at room temperature). The extrapolation of the linear dependence to zero current is defined as T^*. In Fig. 5(b) it is found out that $T^* \sim 490$ K for $W/Co_{0.79}Tb_{0.21}$.

Figure 6(a) shows $R_{\mathrm{AHE}}(i_{\mathrm{pulse}})$ for the $Co_{0.73}Tb_{0.27}$ sample performed for a cryostat temperature of 150 K to highlight the observation of the two switching events. At lower current (37.5 mA), i.e., lower Joule heating effects, we observed up-down current-induced switching polarity while the second one which occurs at a higher current (43 mA) is down-up. This can be understood considering that to achieve the first switching the device reaches a temperature below its $T_{M\,\mathrm{comp}}$, so the sample is still Tb rich and the up-down current-switching polarity observed is as expected [i.e., Fig. 2(h)]. If we continue to increase the intensity of the applied in-plane current pulses, we overcome $T_{M\,\mathrm{comp}}$, and then the perpendicular component of effective torque field $\boldsymbol{H}_{\mathrm{SHE}}$ now changes its sign as discussed previously. Consequently, the second observed switching agrees well for the Co-rich phase (down-up). In Fig. 6(b) the temperature dependence of both switching currents are shown. As discussed, the first (second) switching is congruent with a Tb-rich (Co-rich) current-switching polarity and happens for $T < T_{M\,\mathrm{comp}}$ ($T > T_{M\,\mathrm{comp}}$). The linear extrapolation of both switching currents roughly tends to 350 K (Tb-rich switching) and $T^* \sim 455$ K (Co-rich switching). The value of T^* seems to be slightly higher than T_{switch} [approximately $435\ \mathrm{K} \pm 25$ K, as determined in Fig 4(c)]. We cannot discriminate whether T^* is above or below T_{switch} due to limitations in the analysis. Thus, we believe that our results present alternative perspectives and may encourage continued studies concerning these temperatures. So far, T^* and T_{switch} seem very similar. Nevertheless, the observation that the device always reaches the same temperature when the switching

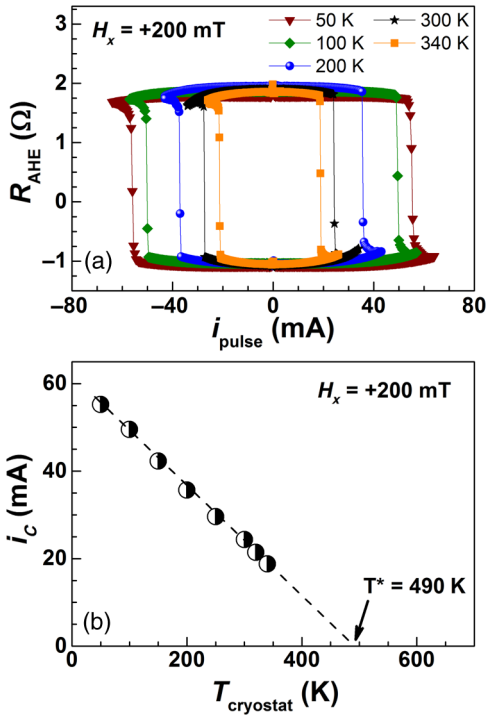

FIG. 5. (a) $R_{\mathrm{AHE}}(i_{\mathrm{pulse}})$ at different cryostat temperatures. Cycles for $x = 0.79$ (Co rich at room temperature). (b) The critical current to reverse M increases linearly when T decreases. The extrapolation of the linear behavior at higher temperature for zero current is defined as T^*.

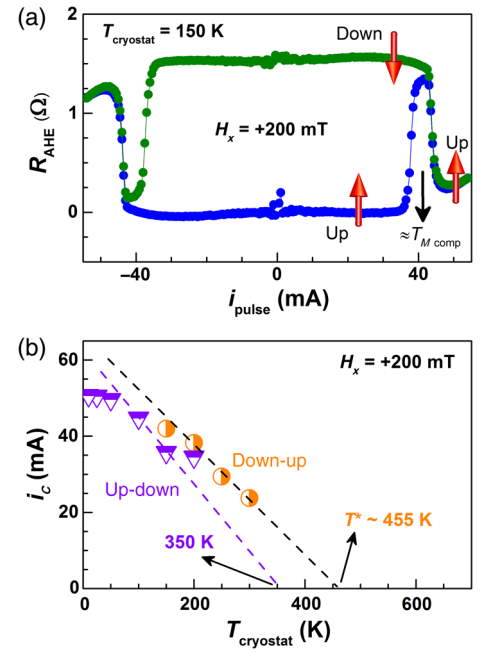

FIG. 6. (a) $R_{\mathrm{AHE}}(i_{\mathrm{pulse}})$ at 150 K for $x = 0.73$ (Tb rich at room temperature). There are two switchings: (i) at lower current it agrees with a Tb-rich-switching polarity (up-down). (ii) The reversal with higher current agrees with a Co-rich-switching polarity (down-up). (b) Temperature dependence of the critical currents for this composition. $T_{M\,\mathrm{comp}}$ would be between 350 and 455 K.

occurs irrespective of the T_{cryo} even without the linear extrapolation has significant implications on the functioning of these devices, and we believe that future studies will have to consider SOT-switching experiments performed about T_{switch} or T^*.

V. *T-x* SWITCHING PHASE DIAGRAM

In Fig. 7(a) the different characteristic temperatures of our W/CoTb systems can be plotted in the (T,x_{Co}) phase diagram. The determined $T_{M\,\mathrm{comp}}$ decreases linearly with the Co concentration as reported for bulk CoTb and thick CoGd films (300 nm) [42,48]. However, T_{switch} and T^* increase linearly with the Co concentration and scale with the Curie temperature T_c, thus depending on composition, and independent of initial temperature. It is remarkable that the T_{switch} and T^* are nearly the same, indicating that, to achieve the switching, one has to reach a specific temperature. The three first questions in Sec. IV are answered. Now let us discuss the physical meaning of these switching temperatures. It is clear that for Co CSP, the temperature of switching is above $T_{M\,\mathrm{comp}}$ and below T_c. Figure 7(a) also shows T_c in bulk CoTb after Hans *et al.* [42].

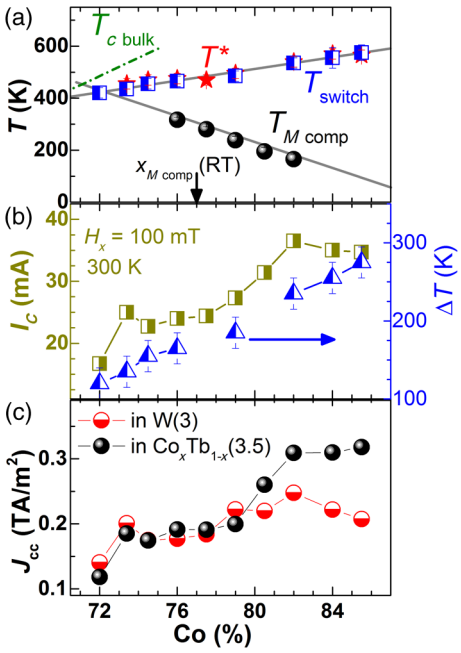

FIG. 7. (a) Characteristic temperatures as function of Co concentration: T^*, T_{switch}, and $T_{M\,\mathrm{comp}}$ independently measured in Hall bar patterned devices (lines are guides for the eyes). It is observed that $T_{M\,\mathrm{comp}}$ follows the same behavior reported for bulk Co_xTb_{1-x} alloys. T^* and T_{switch} have the same trend as that of the Curie temperature T_c. The green dashed line stands for T_c in bulk CoTb after Hans *et al.* [42]. (b) The total critical current injected to reverse M when the experiment is performed at room temperature $(=T_{\mathrm{cryostat}})$, and the variation of temperature $T_{\mathrm{switch}} - T_{\mathrm{cryostat}}$ to reach the switching. (c) The critical current density, calculated from (b), flowing in W and CoTb layers, respectively.

The angular composition temperature $T_{A\,\mathrm{comp}}$ scales with $T_{M\,\mathrm{comp}}$. Indeed, typically $T_{A\,\mathrm{comp}} \sim (T_{M\,\mathrm{comp}} + 30\ \mathrm{K})$ for $Co_{0.775}Gd_{0.225}$ thick films (300 nm) [48]. This is explained by the relationship between the angular moment L, magnetic moment, and the gyromagnetic ratio γ or Landé g factor ($L_{\mathrm{TM,RE}} = M_{\mathrm{TM,RE}}/\gamma_{\mathrm{TM,RE}}$ and $\gamma = g\mu_B/h_b$). Therefore, in CoTb it is expected that the trends of $T_{A\,\mathrm{comp}}$ and $T_{M\,\mathrm{comp}}$ are similar and they decrease with increasing Co concentration as we have shown in Sec. S6 of the Supplemental Material [44,49–54]. However T_{switch} increases with Co concentration, which indicates that T_{switch} is not scaling with $T_{A\,\mathrm{comp}}$ or $T_{M\,\mathrm{comp}}$. For the sake of comparison, we plot the switching current for experiment performed at room temperature together with the temperature increase $\Delta T = T_{\mathrm{switch}} - T_{\mathrm{cryostat}}$, due to the Joule heating effect in Fig. 7(b). We can observe that the temperature is increased between 100 and 300 K. This variation will increase when we reduce T_{cryostat}. Considering that resistivity of both, CoTb and W layers, change similarly with temperature and using the resistivity measured at room temperature we can estimate the critical current density J_{CC} flowing on each layer as displayed in Fig. 7(c). We observe that J_{CC} on W is reduced by a factor of approximately 2 while varying the composition of CoTb. We observe the minimum of J_{CC} at the lower Co concentration measured. This can be explained by the fact that T_C and T_{switch} decrease with decreasing Co concentration. Furthermore, the switching temperature may be understood from thermally excited magnon accumulation in ferrimagnets which vanished when $\partial m/\partial T = 0$ [55]. Thus, T_{switch} would be the critical temperature at which the magnon accumulation signal vanishes, but this correlation needs additional studies.

VI. CONCLUSIONS

In conclusion, we have fully characterized current-induced switching experiments in a series of $//W(3\ \mathrm{nm})/Co_xTb_{1-x}(3.5\ \mathrm{nm})/AlO_x(3\ \mathrm{nm})$ samples. In addition to the SOT effect we demonstrate a strong thermal contribution to achieve the magnetization reversal. For the Co-rich current-switching polarity the device needs to reach the same temperature T_{switch} to achieve the switching. This T_{switch} increases with Co concentration, which then scales with Curie temperature T_c. It is then unlikely that T_{switch} corresponds to angular momentum compensation temperature (which scales with $T_{M\,\mathrm{comp}}$ decreasing with Co concentration). Those results highlight the importance of considering thermal contributions in SOT-switching experiments and the fact that the spin Hall angle determination might be overestimated when thermal contribution is neglected. The use of the resistive W layer increases the heating of the device, reducing strongly the external in-plane needed to assist the SOT. Those results are important for the full understanding of current-induced magnetization switching and may lead the way to alternative technological applications taking advantage of the rather strong heating waste in devices. There is also room to reduce strongly the current density considering the beta phase of W.

ACKNOWLEDGMENTS

This work was supported partly by the French PIA project "Lorraine Université d'Excellence," No. ANR-15-IDEX-04-LUE. By the ANR-NSF Project, No. ANR-13-IS04-0008-01, "COMAG" by the ANR-Labcom Project LSTNM, by project ICEEL Inter-CARNOT OPTICSWITCH. Experiments were performed using equipment from the TUBE—Daum funded by FEDER (EU), ANR, the Region Lorraine, and Grand Nancy. We thank J. Sampaio and S. Petit-Watelot for fruitful discussions and E. Fullerton for a careful reading of the manuscript.

[1] J. E. Hirsch, Spin Hall Effect, Phys. Rev. Lett. **83**, 1834 (1999).
[2] A. Hoffmann, Spin Hall effects in metals, IEEE Trans. Magn. **49**, 5172 (2013).
[3] J. Sinova, S. O. Valenzuela, J. Wunderlich, C. H. Back, and T. Jungwirth, Spin Hall effects, Rev. Mod. Phys. **87**, 1213 (2015).
[4] I. M. Miron, K. Garello, G. Gaudin, P.-J. Zermatten, M. V. Costache, S. Auffret, S. Bandiera, B. Rodmacq, A. Schuhl, and P. Gambardella, Perpendicular switching of a single ferromagnetic layer induced by in-plane current injection, Nature (London) **476**, 189 (2011).
[5] L. Liu, O. J. Lee, T. J. Gudmundsen, D. C. Ralph, and R. A. Buhrman, Current-Induced Switching of Perpendicularly Magnetized Magnetic Layers Using Spin Torque from the Spin Hall Effect, Phys. Rev. Lett. **109**, 096602 (2012).
[6] C. Bi, L. Huang, S. Long, Q. Liu, Z. Yao, L. Li, Z. Huo, L. Pan, and M. Liu, Thermally assisted magnetic switching of a single perpendicularly magnetized layer induced by an in-plane current, Appl. Phys. Lett. **105**, 022407 (2014).
[7] X. Qiu, K. Narayanapillai, Y. Wu, P. Deorani, D.-H. Yang, W. Noh, J. Park, K.-J. Lee, H. Lee, and H. Yang, Spin–orbit-torque engineering via oxygen manipulation, Nat. Nanotechnol. **10**, 333 (2015).
[8] J. C. Rojas-Sánchez, P. Laczkowski, J. Sampaio, S. Collin, K. Bouzehouane, N. Reyren, H. Jaffrès, A. Mougin, and J. M. George, Perpendicular magnetization reversal in $Pt/[Co/Ni]_3/Al$ multilayers via the spin Hall effect of Pt, Appl. Phys. Lett. **108**, 082406 (2016).
[9] D. Wu, G. Yu, Q. Shao, X. Li, H. Wu, K. L. Wong, Z. Zhang, X. Han, P. Khalili Amiri, and K. L. Wang, In-plane current-driven spin-orbit torque switching in perpendicularly magnetized films with enhanced thermal tolerance, Appl. Phys. Lett. **108**, 212406 (2016).
[10] L. Liu, C.-F. Pai, Y. Li, H. W. Tseng, D. C. Ralph, and R. A. Buhrman, Spin-torque switching with the giant spin Hall effect of tantalum, Science **336**, 555 (2012).

[11] C. Zhang, S. Fukami, H. Sato, F. Matsukura, and H. Ohno, Spin-orbit torque induced magnetization switching in nano-scale Ta/CoFeB/MgO, Appl. Phys. Lett. **107**, 012401 (2015).

[12] Y. M. Hung, L. Rehm, G. Wolf, and A. D. Kent, Quasistatic and pulsed current-induced switching with spin-orbit torques in ultrathin films with perpendicular magnetic anisotropy, IEEE Magn. Lett. **6**, 3000504 (2015).

[13] C.-F. Pai, L. Liu, Y. Li, H. W. Tseng, D. C. Ralph, and R. A. Buhrman, Spin transfer torque devices utilizing the giant spin Hall effect of tungsten, Appl. Phys. Lett. **101**, 122404 (2012).

[14] Q. Hao and G. Xiao, Giant Spin Hall Effect and Switching Induced by Spin-Transfer Torque in a W/CoFeB/MgO Structure with Perpendicular Magnetic Anisotropy, Phys. Rev. Applied **3**, 034009 (2015).

[15] S. Cho, S.-H. C. Baek, K.-D. Lee, Y. Jo, and B.-G. Park, Large spin Hall magnetoresistance and its correlation to the spin-orbit torque in W/CoFeB/MgO structures, Sci. Rep. **5**, 14668 (2015).

[16] M. S. Gabor, T. Petrisor, R. B. Mos, A. Mesaros, M. Nasui, M. Belmeguenai, F. Zighem, and C. Tiusan, Spin–orbit torques and magnetization switching in W/Co_2 FeAl/MgO structures, J. Phys. D **49**, 365003 (2016).

[17] J.-C. Rojas-Sánchez, N. Reyren, P. Laczkowski, W. Savero, J.-P. Attané, C. Deranlot, M. Jamet, J.-M. George, L. Vila, and H. Jaffrès, Spin Pumping and Inverse Spin Hall Effect in Platinum: The Essential Role of Spin-Memory Loss at Metallic Interfaces, Phys. Rev. Lett. **112**, 106602 (2014).

[18] W. Zhang, W. Han, X. Jiang, S.-H. Yang, and S. S. P. Parkin, Role of transparency of platinum–ferromagnet interfaces in determining the intrinsic magnitude of the spin Hall effect, Nat. Phys. **11**, 496 (2015).

[19] J. C. Rojas-Sánchez, S. Oyarzún, Y. Fu, A. Marty, C. Vergnaud, S. Gambarelli, L. Vila, M. Jamet, Y. Ohtsubo, A. Taleb-Ibrahimi, P. Le Fèvre, F. Bertran, N. Reyren, J. M. George, and A. Fert, Spin to Charge Conversion at Room Temperature by Spin Pumping into a New Type of Topological Insulator: α-Sn Films, Phys. Rev. Lett. **116**, 096602 (2016).

[20] J. C. Rojas Sánchez, L. Vila, G. Desfonds, S. Gambarelli, J. P. Attané, J. M. De Teresa, C. Magén, and A. Fert, Spin-to-charge conversion using Rashba coupling at the interface between non-magnetic materials, Nat. Commun. **4**, 2944 (2013).

[21] P. M. Haney, H.-W. Lee, K.-J. Lee, A. Manchon, and M. D. Stiles, Current-induced torques and interfacial spin-orbit coupling, Phys. Rev. B **88**, 214417 (2013).

[22] V. P. Amin and M. D. Stiles, Spin transport at interfaces with spin-orbit coupling: Phenomenology, Phys. Rev. B **94**, 104420 (2016).

[23] V. P. Amin and M. D. Stiles, Spin transport at interfaces with spin-orbit coupling: Formalism, Phys. Rev. B **94**, 104419 (2016).

[24] A. Thiaville, S. Rohart, É. Jué, V. Cros, and A. Fert, Dynamics of Dzyaloshinskii domain walls in ultrathin magnetic films, Europhys. Lett. **100**, 57002 (2012).

[25] O. J. Lee, L. Q. Liu, C. F. Pai, Y. Li, H. W. Tseng, P. G. Gowtham, J. P. Park, D. C. Ralph, and R. A. Buhrman, Central role of domain wall depinning for perpendicular magnetization switching driven by spin torque from the spin Hall effect, Phys. Rev. B **89**, 024418 (2014).

[26] C. F. Pai, M. Mann, A. J. Tan, and G. S. D. Beach, Determination of spin torque efficiencies in heterostructures with perpendicular magnetic anisotropy, Phys. Rev. B **93**, 144409 (2016).

[27] N. Mikuszeit, O. Boulle, I. M. Miron, K. Garello, P. Gambardella, G. Gaudin, and L. D. Buda-Prejbeanu, Spin-orbit torque driven chiral magnetization reversal in ultrathin nanostructures, Phys. Rev. B **92**, 144424 (2015).

[28] M. Baumgartner, K. Garello, J. Mendil, C. O. Avci, E. Grimaldi, C. Murer, J. Feng, M. Gabureac, C. Stamm, Y. Acremann, S. Finizio, S. Wintz, J. Raabe, and P. Gambardella, Dynamics driven by spin–orbit torques, Nat. Nanotechnol. **12**, 980 (2017).

[29] K.-S. Lee, S.-W. Lee, B.-C. Min, and K.-J. Lee, Thermally activated switching of perpendicular magnet by spin-orbit spin torque, Appl. Phys. Lett. **104**, 072413 (2014).

[30] K.-S. Lee, S.-W. Lee, B.-C. Min, and K.-J. Lee, Threshold current for switching of a perpendicular magnetic layer induced by spin Hall effect, Appl. Phys. Lett. **102**, 112410 (2013).

[31] N. Roschewsky, T. Matsumura, S. Cheema, F. Hellman, T. Kato, S. Iwata, and S. Salahuddin, Spin-orbit torques in ferrimagnetic GdFeCo Alloys, Appl. Phys. Lett. **109**, 112403 (2016).

[32] K. Ueda, M. Mann, C. Pai, A. Tan, and G. S. D. Beach, Spin-orbit torques in Ta/Tb_xCo_{100-x} ferrimagnetic alloy films with bulk perpendicular magnetic anisotropy, Appl. Phys. Lett. **109**, 232403 (2016).

[33] J. Finley and L. Liu, Spin-Orbit Torque Efficiency in Compensated Ferrimagnetic Cobalt-Terbium Alloys, Phys. Rev. Applied **6**, 054001 (2016).

[34] N. Roschewsky, C. H. Lambert, and S. Salahuddin, Spin-orbit torque switching of ultralarge-thickness ferrimagnetic GdFeCo, Phys. Rev. B **96**, 064406 (2017).

[35] W. S. Ham, S. Kim, D. Kim, K. Kim, T. Okuno, H. Yoshikawa, A. Tsukamoto, T. Moriyama, and T. Ono, Temperature dependence of spin-orbit effective fields in Pt/GdFeCo bilayers, Appl. Phys. Lett. **110**, 242405 (2017).

[36] R. Mishra, J. Yu, X. Qiu, M. Motapothula, T. Venkatesan, and H. Yang, Anomalous Current-Induced Spin Torques in Ferrimagnets near Compensation, Phys. Rev. Lett. **118**, 167201 (2017).

[37] M. Gottwald, M. Hehn, F. Montaigne, D. Lacour, G. Lengaigne, S. Suire, and S. Mangin, Magnetoresistive effects in perpendicularly magnetized Tb-Co alloy based thin films and spin valves, J. Appl. Phys. **111**, 083904 (2012).

[38] S. Mangin, T. Hauet, P. Fischer, D. H. Kim, J. B. Kortright, K. Chesnel, E. Arenholz, and E. E. Fullerton, Influence of interface exchange coupling in perpendicular anisotropy [Pt/Co]50/TbFe bilayers, Phys. Rev. B **78**, 024424 (2008).

[39] C.-H. Lambert, S. Mangin, B. S. D. C. S. Varaprasad, Y. K. Takahashi, M. Hehn, M. Cinchetti, G. Malinowski, K. Hono, Y. Fainman, M. Aeschlimann, and E. E. Fullerton, All-optical control of ferromagnetic thin films and nanostructures, Science **345**, 1337 (2014).

[40] S. Mangin, M. Gottwald, C.-H. Lambert, D. Steil, V. Uhlíř, L. Pang, M. Hehn, S. Alebrand, M. Cinchetti,

G. Malinowski, Y. Fainman, M. Aeschlimann, and E. E. Fullerton, Engineered materials for all-optical helicity-dependent magnetic switching, Nat. Mater. **13**, 286 (2014).

[41] S. Je, J. C. Rojas-Sanchez, T. H. Pham, P. Vallobra, G. Malinowski, D. Lacour, T. Fache, M. Cyrille, D. Kim, S.-B. Choe, M. Belmeguenai, M. Hehn, S. Mangin, G. Gaudin, and O. Boulle, Spin-orbit torque-induced switching in ferrimagnetic alloys: Experiments and modeling, Appl. Phys. Lett. **112**, 062401 (2018).

[42] P. Hansen, C. Clausen, G. Much, M. Rosenkranz, and K. Witter, Magnetic and magneto-optical properties of rare-earth transition-metal alloys containing Gd, Tb, Fe, Co, J. Appl. Phys. **66**, 756 (1989).

[43] S. Alebrand, U. Bierbrauer, M. Hehn, M. Gottwald, O. Schmitt, D. Steil, E. E. Fullerton, S. Mangin, M. Cinchetti, and M. Aeschlimann, Subpicosecond magnetization dynamics in TbCo alloys, Phys. Rev. B **89**, 144404 (2014).

[44] See Supplemental Material at http://link.aps.org/supplemental/10.1103/PhysRevApplied.9.064032 for MOKE and Hall measurements and results, current-induced switching in the full series for $H_x = 100$ mT and 5 mT, power consumption, $H_x - i$ phase diagrams, and estimation of angular compensation temperature.

[45] T. W. Kim and R. J. Gambino, Composition dependence of the Hall effect in amorphous Tb_xCo_{1-x} thin films, J. Appl. Phys. **87**, 1869 (2000).

[46] A. V. Khvalkovskiy, V. Cros, D. Apalkov, V. Nikitin, M. Krounbi, K. A. Zvezdin, A. Anane, J. Grollier, and A. Fert, Matching domain-wall configuration and spin-orbit torques for efficient domain-wall motion, Phys. Rev. B **87**, 020402 (2013).

[47] A. Fert and R. Asomoza, Transport properties of magnetic amorphous alloys, J. Appl. Phys. **50**, 1886 (1979).

[48] M. Binder, A. Weber, O. Mosendz, G. Woltersdorf, M. Izquierdo, I. Neudecker, J. R. Dahn, T. D. Hatchard, J.-U. Thiele, C. H. Back, and M. R. Scheinfein, Magnetization dynamics of the ferrimagnet CoGd near the compensation of magnetization and angular momentum, Phys. Rev. B **74**, 134404 (2006).

[49] Y. Hirata, D. Kim, T. Okuno, T. Nishimura, D. Kim, Y. Futakawa, H. Yoshikawa, A. Tsukamoto, K.-J. Kim, S.-B. Choe, and T. Ono, Correlation between compensation temperatures of magnetization and angular momentum in GdFeCo ferrimagnets, arXiv:1710.07779.

[50] B. D. Cullity and C. D. Graham, *Introduction to Magnetic Materials* (John Wiley & Sons, Inc., Hoboken, New Jersey, 2009), 2nd ed.

[51] W. E. Henry, Saturation magnetization and ferromagnetic interaction in terbium metal, J. Appl. Phys. **30**, S99 (1959).

[52] P. de, V. du Plessis, C. F. van Doorn, and D. C. van Delden, Critical behaviour of helical ordered dysprosium and terbium, J. Magn. Magn. Mater. **40**, 91 (1983).

[53] L. Onsager, A two-dimensional model with an order-disorder transition, Phys. Rev. **65**, 117 (1944).

[54] S. T. Bramwell and P. C. W. Holdsworth, Magnetization and universal sub-critical behaviour in two-dimensional *XY* magnets, J. Phys. Condens. Matter **5**, L53 (1993).

[55] U. Ritzmann, D. Hinzke, and U. Nowak, Thermally induced magnon accumulation in two-sublattice magnets, Phys. Rev. B **95**, 054411 (2017).